Progress in Additive Manufacturing
https://doi.org/10.1007/s40964-024-00577-1

FULL RESEARCH ARTICLE

Prediction of fatigue lifetime and fatigue limit of aluminum parts produced by PBF-LB/M using a statistical defect distribution

Lea Strauß[1] · **Günther Löwisch**[1]

Received: 23 October 2023 / Accepted: 4 February 2024

Abstract
Fatigue tests were performed with samples of AlSi10Mg produced by PBF-LB/M. The failure is caused by inhomogeneities nearby or at the surface of the samples. Therefore, the fatigue strength depends on the crack growth behavior at inhomogeneities under the local stress state at the surface, including residual stresses. For a given size of the failure-causing inhomogeneity, the fatigue lifetime can be described using a crack growth law proposed by Murakami et al. The fatigue limit is given by the threshold value of fatigue crack growth according to the approach of El Haddad. Knowing the distribution of the maximum value of inhomogeneity size in a specimen, it is possible to estimate the S–N curve for 10%, 50%, and 90% crack probability.

Keywords AlSi10Mg · Crack growth · Defect distribution · El Haddad · Fatigue · Residual stress

1 Motivation

Additive manufacturing has made the step from a tool for the production of prototypes to a manufacturing technology for components used in service. Using metallic materials, it is possible to design components capable of withstanding high mechanical loads, including cyclic loads. In such instances, ensuring the longevity and reliability of the product throughout its entire service life cycle necessitates a design approach that guards against fatigue failure. Over the past years, numerous research efforts have been undertaken to comprehend the fatigue behavior of additively manufactured metals [1–8]. Fatigue failure is under among driven by process-induced imperfections. For metal parts produced by a powder bed fusion process using a laser beam (PBF-LB/M) having a machined surface, such imperfections are keyholes, lack of fusion, oxide inclusions, and gas pores. Round gas pores are less harmful compared to oxides, keyholes, and lack of fusion, as these act like a crack, leading to a reduced fatigue strength, especially compared to the theoretical fatigue strength of parts without process-induced defects [7]. Several models exist to describe the fatigue life and fatigue limit of materials with imperfections, mainly based on Murakami's $\sqrt{\text{area}}$-model [4]. It is well proven that these models are valid for additively manufactured materials, especially for the aluminum alloy AlSi10Mg [6–8]. Nevertheless, only a few authors have investigated the influence of mean stress and residual stresses on the fatigue behavior [6], even though the fatigue limit is strongly influenced by residual stresses.

The aim of the work presented here is to determine whether crack growth and crack arrest models are suitable for describing the fatigue strength of additively manufactured specimens when considering the residual stresses in the loading direction. Therefore, results of the fatigue strength of additively manufactured specimens of the aluminum alloy EN AC 43000 (AlSi10Mg) are provided, and two models to predict the lifetime and the fatigue strength are discussed with respect to the distribution of defects and residual stresses.

2 Defect-based models for fatigue life and limit

By now, imperfections of various shapes and sizes are unavoidable for additively manufactured components. Describing the influence of a wide variety of shapes on fatigue strength is challenging. Therefore, it is

✉ Günther Löwisch
guenther.loewisch@unibw.de

[1] Department of Mechanical Engineering, University of the Bundeswehr Munich, Neubiberg, Germany

Published online: 14 March 2024

widely accepted to adopt an approach by Murakami [4]. Murakami simplifies the problem by postulating that the fatigue strength depends on the size of the projected area of the crack-causing defect to a plane perpendicular to the maximum stress direction. This area is easy to measure because the crack surface is also perpendicular to the principal stress direction. The shape of the defect is idealized by a smooth line around the defect. The effect of the defect is considered equivalent to that of a crack with a length of the square root of the area ($\sqrt{\text{area}}$). For a sample loaded with a stress amplitude of σ_a at a load ratio of $R=-1$, the range of the stress intensity ΔK is given by Eq. (1):

$$\Delta K = Y \cdot 2 \cdot \sigma_a \cdot \sqrt{\pi \cdot \sqrt{\text{area}}} \tag{1}$$

The shape factor Y depends on the location of the defect relative to the surface. For defects on or near the surface, it is 0.65; for defects in the volume, it is 0.5. Therefore, defects inside the volume are 30% less critical than those on or near the surface.

Regarding the defects as small cracks, the classic crack growth law can be applied to describe the fatigue life. The crack growth behavior of the material used in this study has not yet been measured, but data for AlSi10Mg can be found in the literature. Nevertheless, there is a simplified model for crack growth behavior proposed by Murakami. Equation (2) describes the growth of a fatigue crack using stress amplitudes instead of ranges of stress intensities [5]. In this equation, the crack size $\sqrt{\text{area}}$ is part of the theoretical fatigue strength σ_w, which is an estimation of the fatigue strength of a specimen with a certain defect size (Eq. (3)).

$$\frac{da}{dN} = C^* \left(\frac{\sigma_a}{\sigma_w} - 1 \right)^{m^*} \sqrt{\text{area}}^{n^*} \tag{2}$$

where C^*, m^*, n^*: parameter of the crack growth law

$$\sigma_w = C \frac{\text{HV} + 120}{\sqrt{\text{area}}^{1/6}} \tag{3}$$

where HV : hardness of the material in Vickers; $C = 1.43$ for defects at the surface, $C = 1.56$ for volume defects

The parameters C*, m*, and n* of Eq. (2) differ from those of the classic crack growth law. They need to be determined by numerical optimization fitting the model to experimental fatigue test results. This crack growth model only applies for loadings in the high cycle fatigue (HCF) regime, leading to a fatigue life between approximately 50,000 and 500,000 cycles. At higher loads, the plastic deformation at the crack tip needs to be considered, which is not the aim of this work. For stress amplitudes below the HCF range, crack arrest and thus runouts can occur if the range of stress intensity at the crack tip is below the threshold value for crack propagation.

For long cracks, the threshold value for crack growth is the material constant $\Delta K_{\text{th-LC}}$. In the Kitagawa–Takahashi diagram [9], a plot of the fatigue strength against the crack size, the material constant $\Delta K_{\text{th-LC}}$ leads to a straight line with the slope $\sqrt{2}$, when logarithmic scales are used. Crack sizes above this line represent cracks leading to failure; crack sizes below represent a crack arrest. Romano and Beretta [7] give a value of $\Delta K_{\text{th-LC}} = 3.25\ \text{MPa}\sqrt{\text{m}}$ for PBF-LB/M/AlSi10Mg (Fig. 1, line (1)). For physically short cracks, the threshold value depends on the crack size. It gets smaller as the crack length decreases. Very short cracks no longer have any influence on the fatigue strength, resulting in a fatigue limit similar to the fatigue limit of a specimen without defects, represented by a horizontal line in the Kitagawa–Takahashi diagram (Fig. 1, line (2)). Murakami suggests to estimate the fatigue limit of a defect-free specimen by 1.6 times the Vickers hardness [4]. For example, for a material with a hardness of 123 HV, a fatigue limit of 196 MPa is obtained at a stress ratio of $R=-1$. The lines (1) and (2) intersect at a crack length of $a_0 = 52$ µm (Fig. 1, line (3)). However, the transition from one line to the other is not a sharp edge. As mentioned earlier, for small cracks or defects, the crack growth threshold depends on the crack size. The most common approach to describe this transition area is Eq. (4) of El Haddad [10] (Fig. 1, line (4)):

$$\Delta K_{\text{th}} = Y \cdot 2\sigma_{f(a)} \sqrt{\pi (a + a_0)} \tag{4}$$

where ΔK_{th} : threshold value for fatigue crack growth, depending on defect size

$\sigma_{f(a)}$: fatigue strength of a sample with a defect of size a,

a : defect size, here equal to $\sqrt{\text{area}}$

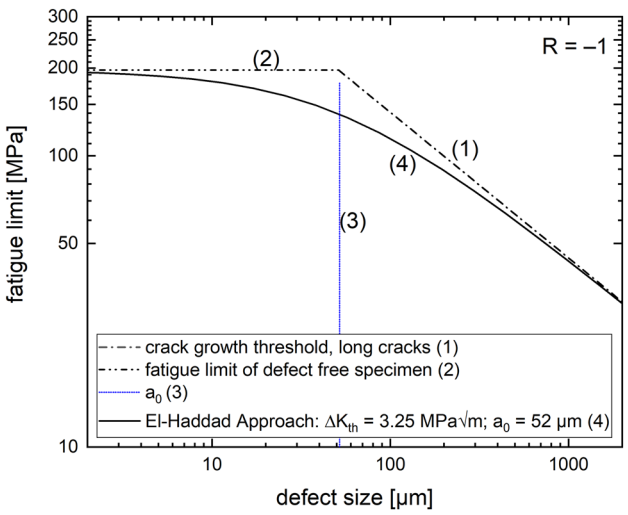

Fig. 1 Kitagawa–Takahashi diagram for PBF-LB/M/AlSi10Mg, using data from literature [4, 7]

For a specimen with a known size of the most critical defect, the relating fatigue limit can be read at the El Haddad line. Failure occurs at loads above the line. A load below the line results in a runout. This model is, therefore, suitable for describing fatigue strength.

3 Experimental setup

Specimens made from the material AlSi10Mg were used for the fatigue tests. Fatigue samples were manufactured by the PBF-LB/M process using a SLM 125 (SLM Solutions Group) machine. The commercial powder used had a grain size from 20 µm up to 60 µm. Table 1 summarizes the manufacturing parameters. After printing, the samples were machined to their final shape (technical drawing and a photograph in Fig. 2). The rough surface after the printing process, therefore, has no influence on fatigue strength.

The residual stresses at the surface of the specimens were measured by X-ray diffraction according to the standard EN 15305. For this, a D8 Discover X-ray diffraction machine (Bruker Corporation) was used. Residual stress was measured at three distinct spots within the testing area and at three different samples. At every spot, the residual stresses were measured in 0°, 45°, and 90° direction relative to the specimen's axis to obtain the complete residual stress tensor at the surface. The mean value of all measurements was + 44 MPa in build direction and + 54 MPa perpendicular to the specimen's axis. It is known from literature that the depth of the residual stress in AlSi10Mg PBF-LB induced due to machining is about 100 µm [6].

Fatigue testing was performed using different stress ratios ($R = -1$ and $R = 0.1$), and rotating bending at a stress ratio of $R = -1$. For rotating bending, the diameter of the specimens in the test section was increased from 8 to 9 mm. Tensile–compression tests were performed using a servo hydraulic testing machine 5001 (Instron) with a capacity of 50 kN. The test frequency was set to 35 Hz. The rotating bending tests were conducted using a Rotabend (Sincotec)

Table 1 Printing parameters for all PBF-LB/M/AlSi10Mg fatigue specimens

Parameter	Value
Building direction	Vertical
Laser power	350 W
Scanning speed	1650 mm/s
Layer height	30 µm
Hatch distance	130 µm
Preheating of building plate	150 °C
Scan strategy	Rotating scan pattern

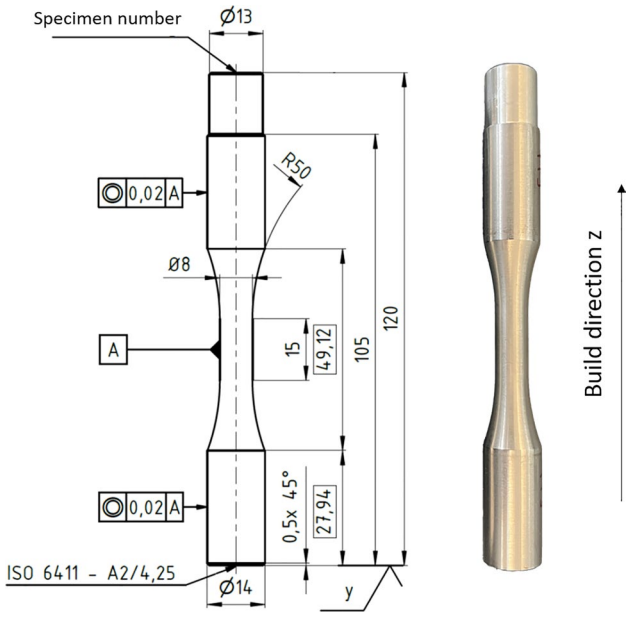

Fig. 2 Specimen for fatigue tests (tensile–compression tests and pure tension). All dimensions in mm

rotating bending machine with a capacity of 50 Nm. The tests were run with a frequency of 100 Hz. After 10^7 cycles without failure, the test was stopped and the specimen was declared as a runout.

At least 40 fatigue tests were tested to obtain 1 S–N curve. Afterward, all broken specimens were investigated by a digital light microscope VHX 7000 (Keyence) to detect the origin of the fatigue crack at the crack surface, and to measure the size of each crack-initiating defect.

4 Results

4.1 S–N curves

In addition to a number of pre-tests, fatigue tests were performed at various stress amplitude levels for different loading conditions (see Figs. 3 and 4), where the upper two amplitudes describe the high cycle fatigue (HCF) regime. In this regime, all specimens broke. The slope and position of the median S–N curve, along with the standard deviation of the results, were calculated using the pearl string method for the HCF regime. The standard deviation can be used to calculate S–N curves for 10% or 90% crack probability, respectively. This method is detailed in DIN 50100 [11] and by Masendorf and Müller [12].

The stress amplitudes below the HCF regime were utilized to determine the fatigue limit. For these stress amplitude levels, including runouts, the crack probability was calculated for every level. By fitting the crack probability

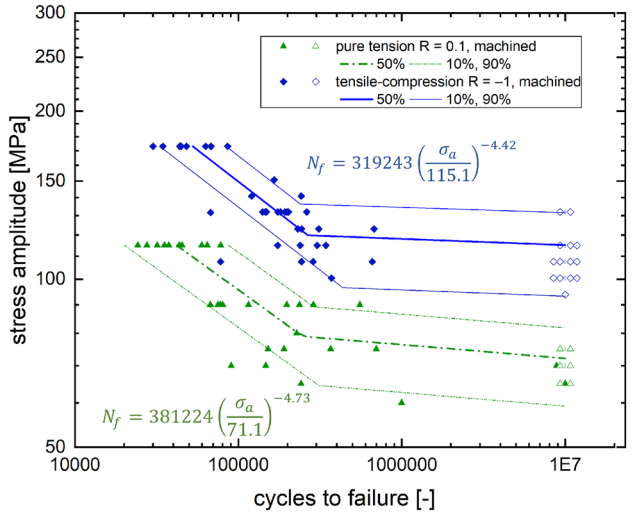

Fig. 3 S–N curves at tensile–compression ($R=-1$) and pure tension ($R=0.1$). Open symbols represent runouts

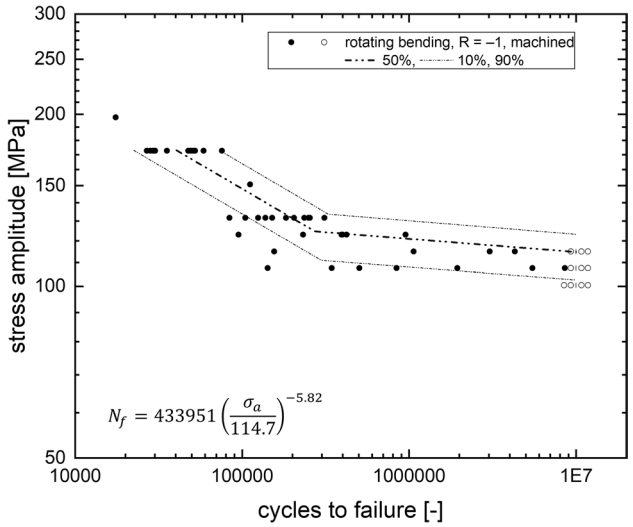

Fig. 4 S–N curve for rotating bending ($R=-1$). Open symbols represent runouts

versus the stress levels using a Weibull distribution, the 50%, 10%, and 90% fatigue limit were determined. Overall, fatigue tests exhibited a big scatter in the results.

The fatigue limit at the stress ratio $R=0.1$ (72 MPa) is lower than under reversed tension–compression with $R=-1$ (115 MPa), which is caused by the additional mean stress at $R=0.1$. The mean stress at $R=-1$ is zero, but one has to consider the residual stress acting as a mean stress as well. As the residual stress in build direction is positive (+44 MPa), it reduces the fatigue strength of the samples. For $R=0.1$, the mean stress of the fatigue limit is 88 MPa. Adding the residual stresses of +44 MPa, the acting total mean stress is 132 MPa. Figure 5 shows both data points

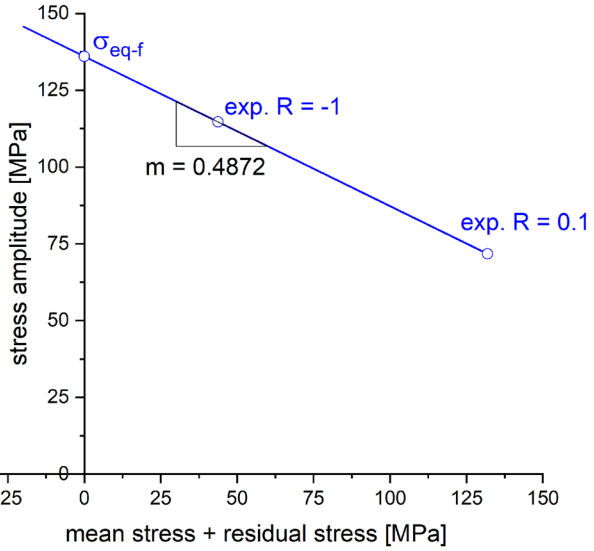

Fig. 5 Haigh diagram: influence of the mean stress on the fatigue limit, considering residual stresses for PBF-LB/M/AlSi10Mg

in a Haigh diagram, where the effect of the mean stress to the stress amplitude is depicted. The slope line between the two measured data points is the mean stress sensitivity m, calculated to 0.4872. Extrapolating the connecting line to a mean stress of zero shows that for a specimen without residual stresses, the fatigue limit under tensile–compression loading is 136 MPa. In this paper, this calculated fatigue limit will be referred to as the equivalent fatigue limit $\sigma_{eq\text{-}f}$.

There are a number of other models to describe the influence of mean stresses on fatigue strength [13, 14]. As the mean stress sensitivity according to Haigh is the simplest method, it is used in this paper.

In accordance with the Haigh diagram, it is possible to reevaluate the loading conditions of a specimen. This involves the nominal stress amplitude (σ_a), mean stress (σ_m), and surface residual stress (σ_r). Through recalculation, an equivalent stress amplitude (σ_{eq}) can be determined:

$$\sigma_{eq} = \sigma_a + m\left(\sigma_m + \sigma_r\right) \tag{5}$$

The equivalent stress amplitude makes the S–N curves with different mean stress and residual stress comparable. The results of all fatigue tests are compared in this way in Fig. 6. Although there is a stress gradient with rotating bending loading, the results under tensile–compression loading and under rotating bending loading fall within the same scatter band. Nevertheless, the scatter of the fatigue test result is relatively large. One possible reason for this scatter may be the varying size of each crack-initiating defect.

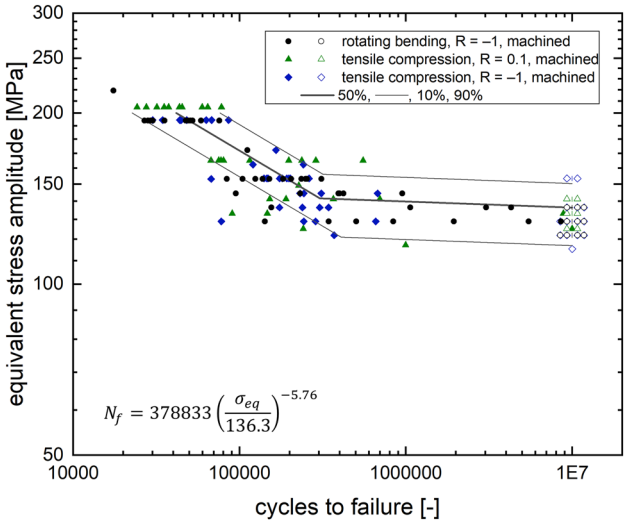

Fig. 6 Comparison of the S–N curves for different loading conditions, using the equivalent stress amplitude

4.2 Defect distribution

The investigation of the crack surfaces yields two main results. First, all observed cracks started from a defect, which was either lack of fusion or keyhole. An example is provided in Fig. 7. Second, the crack-initiating defect is always directly at or near the original surface. This is in accordance with the form factor Y in Eq. (1), which leads to a fatigue limit 30% higher at the surface than in the volume.

It is reasonable to assume that the defect causing failure is typically the largest defect located at or near the surface of a specimen. By sorting the measured crack-initiating defects based on their $\sqrt{\text{area}}$ size, one can obtain a maximum value distribution of these defects. A distribution of the maximum defect in a cumulative probability plot using a Gumbel distribution is shown in Fig. 8 for the tensile–compression loaded specimens with $R=-1$. The crack-initiating defects had a size between 36 µm and 184 µm. The plot shows that at 50% of the specimens, the size of the failure-causing defect is 80 µm or smaller. At 90% of the specimens, the maximum defect is smaller than 129 µm, and at 10% of the specimens, the failure-causing defect was 48 µm or smaller.

In Fig. 9, the influence of the defect size on the lifetime of the specimens is shown for three different stress amplitudes. Since the S–N curves of samples loaded with $R=-1$ are comparable for tensile–compression and rotating bending, measured defect sizes are consolidated. In the logarithmic scale, there is a clear linear correlation between the size of the crack-initiating defect and the cycles to failure. Nevertheless, there is a scatter around the regression line, which is outstandingly larger for the lowest stress amplitude of 129 MPa. However, the stress amplitude of 129 MPa is close to the fatigue limit. Another seven specimens tested at this amplitude were runouts, for which the size of the most damaging defect is not known and, therefore, cannot be shown in the plot.

5 Discussion

5.1 Crack growth model for fatigue life

The fatigue failure is under among driven by the process-induced defects. Regarding the defects as small cracks, one can use Eq. (2) to describe the fatigue life. The results under tensile–compression loading at nominal stress amplitudes of 173 MPa ($\sigma_{eq}=194$ MPa) resp. 132 MPa ($\sigma_{eq}=153$ MPa) were used to determine the parameters C*, m*, and

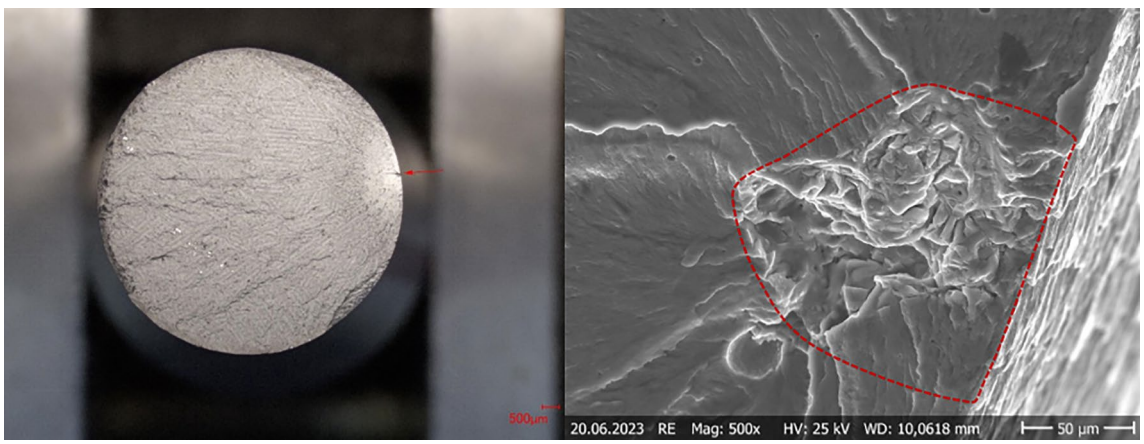

Fig. 7 Crack surface of a specimen with $\sigma_a=173$ MPa, tensile–compression loading with $R=-1$, $N_f=30{,}800$ cycles. The macroscopic image (left) shows the origin of the crack, red arrow. The SEM picture (right) shows the initiating defect, a keyhole. The area of the defect is marked by a red dashed line. The size of the crack-initiating defect is $\sqrt{\text{area}}=117$ µm

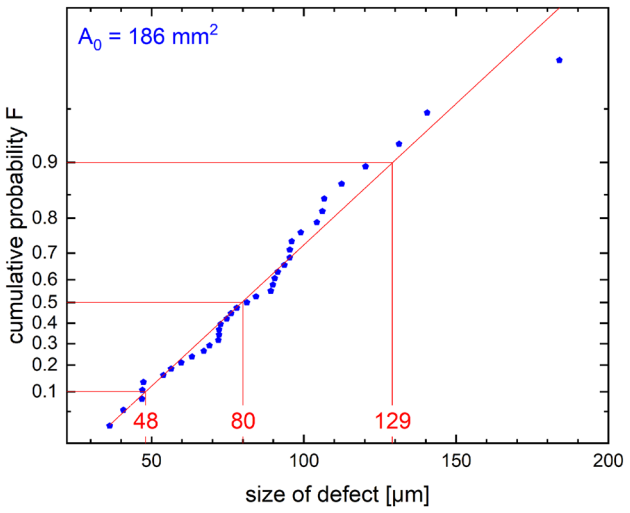

Fig. 8 Maximum value distribution of the crack-initiating defect size $\sqrt{\text{area}}$ of the specimens loaded with tensile–compression at $R=-1$

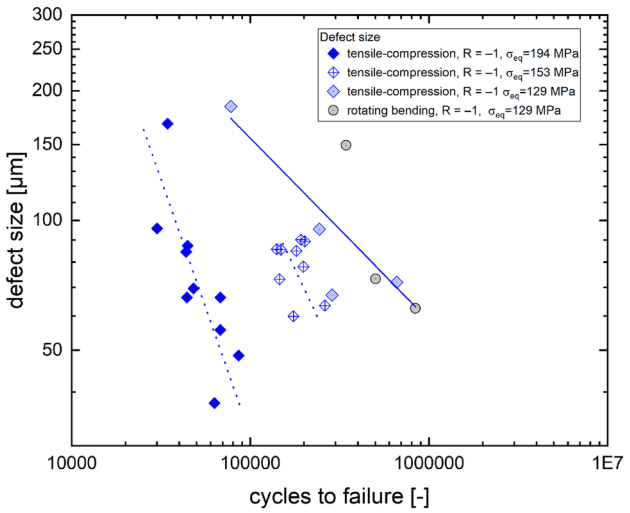

Fig. 9 Influence of the defect size $\sqrt{\text{area}}$ on the fatigue life

n* through numerical optimization. The results are given in Table 2, where the second column shows the parameters obtained when using the nominal stress amplitude and the third column when using the equivalent stress amplitude instead.

The lifetimes calculated using the parameters for the nominal stress are compared in Fig. 10 with the experimental lifetimes of the samples used for the optimization.

The match is quite accurate but there is still some remaining scatter. This variability may be caused by other influencing parameters besides the defect size, such as local differences in microstructure and residual stresses.

Furthermore, the lifetime of theoretical specimens with a defect size of 48 µm, 80 µm, and 129 µm (crack size at a

Table 2 Calculated parameters C*, m*, and n* for the crack growth law (Eq. (2)) determined by numerical optimization, using the results of the fatigue tests at 173 MPa and 132 MPa nominal stress amplitudes of the tensile–compression tests ($R=-1$)

Parameter	Using nominal stress	Using equivalent stress
$C * \left[\frac{1}{\text{cycle}} \frac{\mu m}{\mu m^{n^*}}\right]$	$4.5\ 10^{-5}$	$4.5\ 10^{-5}$
m* [−]	2	2.7
n* [−]	1	0.88

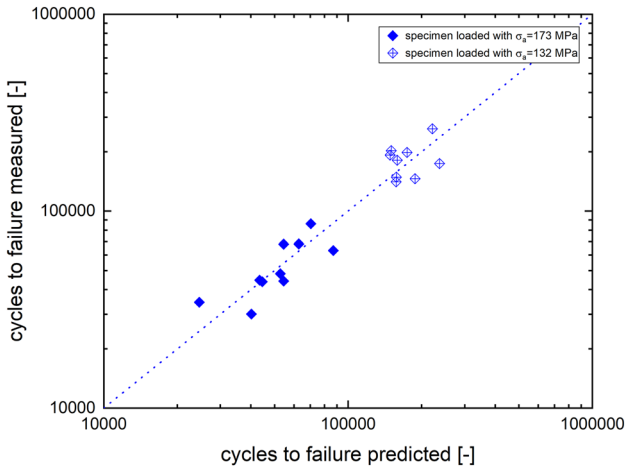

Fig. 10 Experimental measured lifetime of fatigue specimens under tensile–compression loading (dots), compared with the estimated lifetime (line) using the crack growth model (Eq. (2)) with the parameter set in Table 2 (second column) and the particular size of the failure-causing defect

failure probability of 10%, 50%, and 90%) was calculated at different stress amplitudes using Eq. (2) and the values in Table 2, second column. This results in a prediction of the S–N curve for a specimen with the given defect size being the maximum defect in 10%, 50%, and 90% of the specimens. These lines are plotted in Fig. 11 as red lines. For the HCF regime, they exhibit a good correlation with the experimentally determined 10%, 50%, and 90% S–N curves of the tensile–compression tests.

The parameters using the nominal stress amplitude are only valid for the tensile–compression tests, as residual stresses are not considered as influencing factors. Using the parameter set for the equivalent stress amplitude (third column in Table 2) and therefore considering the present mean and residual stresses, the fatigue life prediction can be applied to all fatigue tests presented in this paper (see Fig. 12). Once again, the correlation to the experimentally determined S–N curves is good. The estimated lifetime for a defect with an 80 µm size corresponds well with the S–N

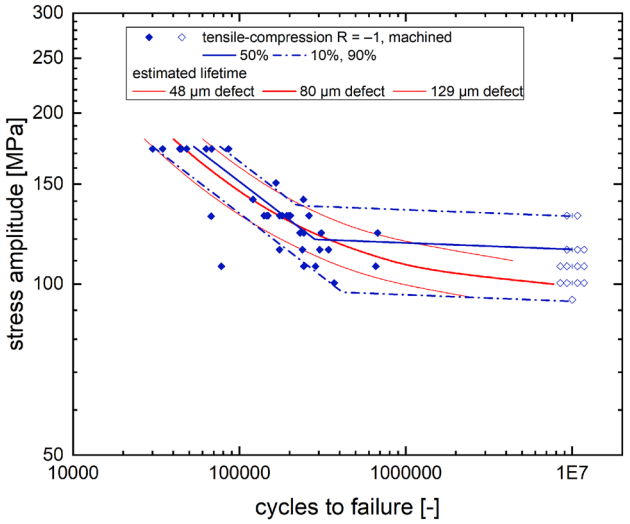

Fig. 11 Predicted lifetime for tensile–compression loading (red) of the tested fatigue specimens with the experimentally determined S–N curves (blue) and each relating tested fatigue sample (dots), using nominal stresses

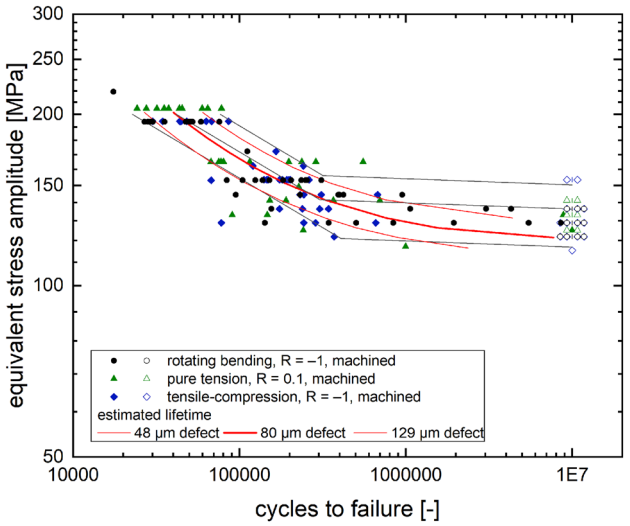

Fig. 12 Predicted lifetime (red lines) for fatigue samples loaded with rotating bending ($R=-1$, black dots), tensile–compression ($R=-1$, blue squares), and pure tension ($R=0.1$, green triangles), using equivalent stresses considering mean and residual stresses. For comparison, experimentally determined 10%, 50%, and 90% crack probability S–N curves are depicted (black lines). Open symbols represent runouts

curve for a 50% crack probability, and the estimated lifetime for a defect with a 129 µm size corresponds to the 10% crack probability line. Despite this, the lifetime for specimens with small defects of 49 µm is slightly underestimated compared to the S–N curve for 90% crack probability. Nevertheless, the crack growth law given in Eq. (2) is suitable to describe the fatigue lifetime of specimens under cyclic loading.

Nevertheless, Eq. (2) is not suitable for describing the fatigue limit, which is underestimated by Eq. (2), as seen in Figs. 11 and 12. Equation (2) is based on crack growth laws for physically long cracks. In the regime of fatigue strength, one has to consider crack arrest effects, which are not accounted for in Eq. (2).

5.2 Crack arrest model for fatigue limit

Murakami et al. showed that the fatigue limit depends on the threshold value for crack growth of the material used [4]. As discussed in Sect. 2, the El Haddad approach describes the threshold values depending on the defect size in the Kitagawa–Takahashi diagram. Indeed, the size of the defects causing fatigue failure is between 36 µm and 184 µm, which is within the area of transition from long crack growth to the fatigue limit of a defect-free specimen. Figure 13 shows the Kitagawa–Takahashi diagram, with the El Haddad approach depicted as solid line. For a specimen with a given defect size, one expects failure when the load amplitude is above the El Haddad line and a runout when it is below.

For all specimens under tensile–compression loading (nominal $R=-1$), which failed at a stress amplitude between 100 and 140 MPa, the corresponding stress amplitude and defect size are plotted. As all of these samples cracked, they should be located above the El Haddad line, meaning in the region of failure. However, nearly half of the tested fatigue specimens did not fit this criterion. This may be caused by the positive residual stresses at the specimen's surface, which reduce the fatigue limit. Residual stresses act as a mean stress, but the Kitagawa–Takahashi diagram used is

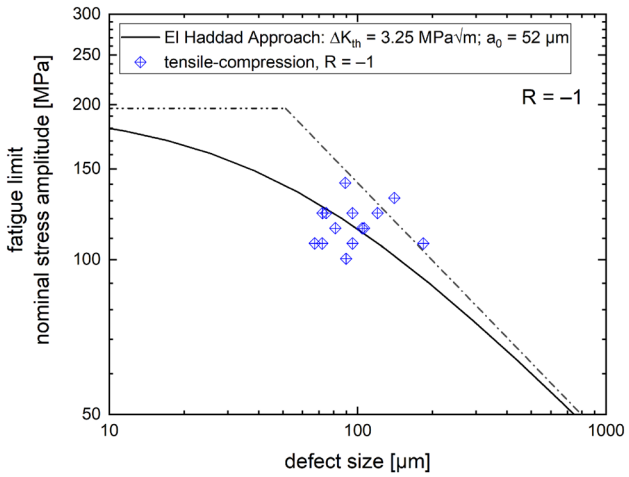

Fig. 13 Kitagawa–Takahashi diagram for PBF-LB/M/AlSi10Mg (see also Fig. 1). Markers represent the size of defects leading to fatigue failure for tested specimens broken under tensile–compression loading using nominal stress amplitude. The fatigue life prediction according to El Haddad is depicted as solid line

valid only for $R=-1$, a loading condition without a mean stress.

Considering the residual stress using the equivalent stress amplitude as in Eq. (5), the data are recalculated to $R=-1$, a loading condition without mean stress. Calculating the equivalent stress amplitude, results under rotating bending, pure tension, and tensile–compression are comparable. All fatigue test results obtained in the region of the fatigue limit are plotted in Fig. 14. Besides two test specimens under pure tension, all results are directly on the El Haddad line or above, where they are expected as broken test specimens. Therefore, the value of 3.25 MPa$\sqrt{\text{m}}$ describes the experimental data quite well.

.

The fatigue limit at a crack size of 48 µm, 80 µm, and 129 µm, as indicated by the El Haddad line, represents the fatigue limit at 10%, 50%, and 90% crack probability, respectively. In Table 3, this theoretically estimated fatigue limit is compared to the experimentally determined fatigue limit.

The experimentally determined fatigue limits at a crack probability of 10%, 50%, and 90% are approximately 10 MPa higher than the estimated fatigue limits. Therefore, the presented estimation is conservative. This difference might be caused by the parameters of the El Haddad line used, which are obtained from the literature and do not necessarily have to be the parameters of the material reported in the paper.

By adjusting the parameters a_0 and ΔK_{th}, the El Haddad line can be shifted that the predicted fatigue strengths for 10%, 50%, and 90% fracture probability correspond to the experimental results. The change in the ΔK_{th} value required for this is no greater than the spread of threshold value measurements from two different sample batches on two different machines. The resulting adjusted El Haddad line is shown as a red line in Fig. 15.

Applying this adjustment, more data lay left or below of the new El Haddad line, the area where no failure is expected. Therefore, even though the new line describes the fatigue limit correct, there are specimens broken with a defect size, which should not lead to a failure at the applied stress amplitude. Based on these results, it is evident that the El Haddad line is not a sharp border between failure and runout. Instead, the El Haddad line describes the influence of the size of a defect on the fatigue limit, possibly affected by other factors like local differences in microstructure or local residual stresses. Consequently, there should be also defects located in the area left of the El Haddad line, which do not lead to failure, because the local microstructure is less detrimental.

Table 3 Estimated and experimental measured fatigue limit at a crack probability of 10%, 50%, and 90%

Crack probability	Estimated fatigue limit	Fatigue limit experimental
10%	106 MPa	116.9 MPa
50%	123 MPa	136.3 MPa
90%	141 MPa	150.3 MPa

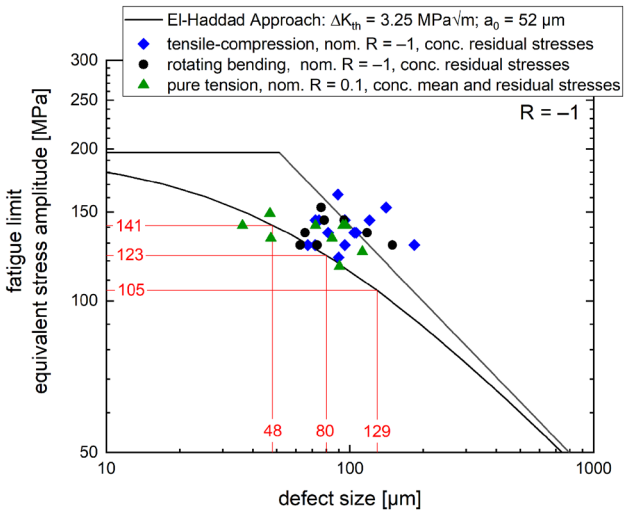

Fig. 14 Kitagawa–Takahashi diagram for PBF-LB/M/AlSi10Mg. The size of the crack-initiating defect is shown by the data points for broken samples. For runouts, the size of the most damaging defect is unknown. The red lines indicate the 10%, 50%, and 90% fatigue strength expected from the defect size distribution

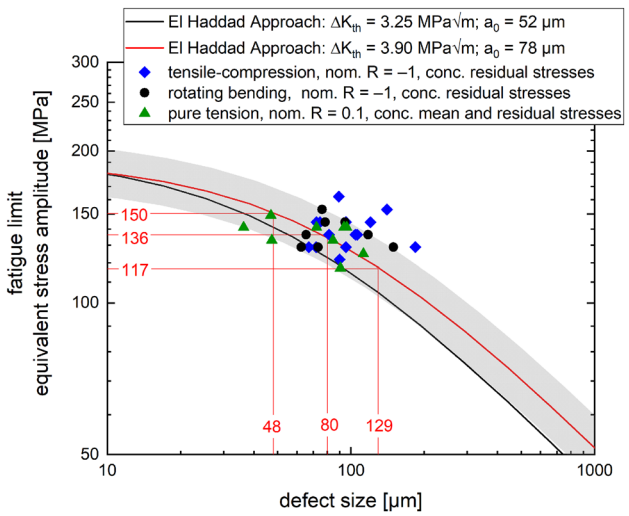

Fig. 15 Fitted El Haddad line in the Kitagawa–Takahashi diagram for PBF-LB/M/AlSi10Mg

6 Conclusion and outlook

This study focused on the prediction of fatigue lifetime and fatigue limit of PBF-LB/M/AlSi10Mg using a statistical defect distribution. To achieve this, S–N curves of fatigue samples with a machined surface, tested at different load ratios and fatigue testing principles, were assessed. For the evaluation of the investigated fatigue specimens, a Kitagawa–Takahashi diagram was used. In this context, the approach by El Haddad was employed to describe the transition between crack propagating and non-propagating process-induced defect. To further consider the existing residual stresses as well as mean stresses, an equivalent stress was defined.

The findings showed that the fatigue strength of additively manufactured AlSi10Mg is mainly driven by process-induced defects in samples with a machined surface. Simple crack growth and crack arrest models, respectively, can describe the influence of these defects. Some scatter might persist due to the influence of local differences in microstructure and residual stresses. However, it is possible to predict the fatigue limit and the fatigue lifetime when the distribution of the defect size and the global residual stress state in a specimen are known.

To expand the method to a more general useful tool, further tasks are remaining:

- A more thorough examination of the impact of mean stresses and residual stresses is warranted. In this paper, they are rated as similar. However, residual stress may relax during cyclic loading, leading to a reduced influence on the fatigue limit. Therefore, further work has to be done to describe the influence of residual stresses in more detail.
- Using the equivalent stress amplitude was a useful tool to compare loadings with different mean stresses. Nevertheless, there are a number of models to describe the influence of mean stresses on the crack growth behavior, which should be compared as well.
- For additively manufactured materials, an anisotropic behavior is known. The presented experiments were performed with vertically samples built only, leading to a crack path parallel to the layering. Samples built horizontally or under 45° will show another crack growth behavior, leading to different results.
- Finally, the investigation should be conducted again using heat-treated specimens. It is already known that a heat treatment following the additive manufacturing process reduces the scatter of fatigue tests significantly [15]. Conducting heat treatment of an entire specimen yields a more homogenous microstructure compared to a generative building process with a local time history within the specimen like PBF-LB/M. Also, the local residual stresses would be decreased and homogenized. One can assume that heat-treated specimens exhibit a smaller dispersion around the El Haddad line than the specimens used in this investigation with an as-built microstructure.

Funding Open Access funding enabled and organized by Projekt DEAL. This research is part of the project FLAB-3Dprint and funded by dtec.bw—Digitalization and Technology Research Center of the Bundeswehr which we gratefully acknowledge. dtec.bw is funded by the European Union—NextGenerationEU.

Declarations

Conflict of interest For this research, there is no conflict of interest for all authors.

References

1. Tenkamp J, Stern F, Walther F (2022) Uniform fatigue damage tolerance assessment for additively manufactured and cast Al-Si alloys: an elastic-plastic fracture mechanical approach. Addit Manuf Lett 3:100054. https://doi.org/10.1016/j.addlet.2022.100054
2. Blinn B, Ley M, Buschhorn N, Teutsch R, Beck T (2019) Investigation of the anisotropic fatigue behavior of additively manufactured structures made of AISI 316L with short-time procedures PhyBaLLIT and PhyBaLCHT. Int J Fatigue 124:389–399. https://doi.org/10.1016/j.ijfatigue.2019.03.022
3. Strauß L, Löwisch G (2023) Effect of residual stress, surface roughness and porosity on fatigue life of PBF-LB AlSi10Mg [Accepted]. Adv Struct Mater
4. Murakami Y (2019) Metal fatigue: effects of small defects and nonmetallic inclusions. Academic Press, London
5. Murakami Y, Takagi T, Wada K, Matsunaga H (2021) Essential structure of S-N curve: prediction of fatigue life and fatigue limit of defective materials and nature of scatter. Int J Fatigue. https://doi.org/10.1016/j.ijfatigue.2020.106138
6. Sausto F, Tezzele C, Beretta S (2022) Analysis of fatigue strength of L-PBF AlSi10Mg with different surface post-processes: effect of residual stresses. Metals 12:898. https://doi.org/10.3390/met12060898
7. Romano S, Brückner-Foit A, Brandão A, Gumpinger J, Ghidini T, Beretta S (2018) Fatigue properties of AlSi10Mg obtained by

additive manufacturing: defect-based modelling and prediction of fatigue strength. Eng Fract Mech 187:165–189. https://doi.org/10.1016/j.engfracmech.2017.11.002
8. Rhein RK, Shi Q, Arjun Tekalur S, Wayne Jones J, Carroll JW (2021) Effect of direct metal laser sintering build parameters on defects and ultrasonic fatigue performance of additively manufactured AlSi10Mg. Fatigue Fract Eng Mater Struct 44:295–305. https://doi.org/10.1111/ffe.13355
9. Aigner R, Pusterhofer S, Pomberger S, Leitner M, Stoschka M (2019) A probabilistic Kitagawa-Takahashi diagram for fatigue strength assessment of cast aluminium alloys. Mater Sci Eng A 745:326–334. https://doi.org/10.1016/j.msea.2018.12.108
10. El Haddad MH, Topper TH, Smith KN (1979) Prediction of non-propagating cracks. Eng Fract Mech 11(573):584
11. DIN 50100 (2022) Schwingfestigkeitsversuch - Durchführung und Auswertung von zyklischen Versuchen mit konstanter Lastamplitude für metallische Werkstoffproben und Bauteile. Beuth-Verlag, Berlin. https://doi.org/10.31030/3337109
12. Masendorf R, Müller C (2018) Execution and evaluation of cyclic tests at constant load amplitudes – DIN 50100:2016: dedicated to Professor Dr.-Ing. Harald Zenner on the occasion of his eightieth birthday. Mater Test 60(10):961–968. https://doi.org/10.3139/120.111238
13. Dowling NE, Calhoun CA, Arcari A (2009) Mean stress effects in stress-life fatigue and the Walker equation. Fatigue Fract Eng Mat Struct 32(3):163–179. https://doi.org/10.1111/j.1460-2695.2008.01322.x
14. Newman JC Jr (1984) A crack opening stress equation for fatigue crack growth. Int J Fract. https://doi.org/10.1007/BF00020751
15. König K, Görres F, Lübbecke S, Löwisch G, Brenner S, Nedeljkovic-Groha V (2020) Versagen gedruckter Proben aus AlSi10Mg unter zyklischer Beanspruchung. 5. Tagung des DVM-Arbeitskreises Additiv gefertigte Bauteile und Strukturen 2020. https://doi.org/10.48447/ADD-2020-005